Characteristics and generation of elastic turbulence in a three-dimensional parallel plate channel using direct numerical simulation*

Hong-Na Zhang(张红娜)[1], Feng-Chen Li(李凤臣)[1], Xiao-Bin Li(李小斌)[1,†], Dong-Yang Li(李东阳)[1], Wei-Hua Cai(蔡伟华)[1,‡], and Bo Yu(宇波)[2]

[1] *School of Energy Science and Engineering, Harbin Institute of Technology, Harbin* 150001, *China*
[2] *Beijing Institute of Petrochemical Technology, Beijing* 102617, *China*

(Received 18 March 2016; revised manuscript received 19 April 2016; published online 2 August 2016)

Direct numerical simulations (DNSs) of purely elastic turbulence in rectilinear shear flows in a three-dimensional (3D) parallel plate channel were carried out, by which numerical databases were established. Based on the numerical databases, the present paper analyzed the structural and statistical characteristics of the elastic turbulence including flow patterns, the wall effect on the turbulent kinetic energy spectrum, and the local relationship between the flow motion and the microstructures' behavior. Moreover, to address the underlying physical mechanism of elastic turbulence, its generation was presented in terms of the global energy budget. The results showed that the flow structures in elastic turbulence were 3D with spatial scales on the order of the geometrical characteristic length, and vortex tubes were more likely to be embedded in the regions where the polymers were strongly stretched. In addition, the patterns of microstructures' elongation behave like a filament. From the results of the turbulent kinetic energy budget, it was found that the continuous energy releasing from the polymers into the main flow was the main source of the generation and maintenance of the elastic turbulent status.

Keywords: elastic turbulence, viscoelastic fluid, direct numerical simulation, rectilinear shear flow

PACS: 47.20.Gv, 47.27.ek, 47.27.Cn **DOI:** 10.1088/1674-1056/25/9/094701

1. Introduction

The rheological properties of the Newtonian fluid could be significantly modified by the addition of a small amount of flexible microstructures such as polymers or some surfactant additives, and the fluid turns to a viscoelastic one. Compared with the Newtonian fluid flow, two kinds of nonlinearity exist in viscoelastic fluid flow, which are nonlinear inertial and nonlinear elastic effects, but do not necessarily coexist.[1] As a result, a variety of different flow regimes turn up due to the additional elastic nonlinearity, depending on the feedback of microstructures on the main flow. The feedback is actually decided by microstructure status such as in a coiled or stretched configuration. For viscoelastic fluid flow , besides the well-known Reynolds number Re, the Weissenberg number Wi is another important dimensionless parameter and describes the competition between polymer stretching by main flow and microstructure relaxation by itself. For cases with $Wi \ll 1$, microstructures relax much faster than the main flow stretching, and thus they are always in a coiled state and embedded passively in the flow. In these cases, the feedback of microstructures on the flow could be ignored. However, for cases with Wi on the order of unity or larger, the striking feedback will be induced because of the significant growth of microstructure length. For example, the substantial reduction of turbulent drag resistance occurs in the inertial turbulent flow when inertial and elastic nonlinearity coexist[2] and has attracted numerous researchers.[3–7] On the other hand, at an arbitrarily low Reynolds number, with solely elastic nonlinearity the flow instability and even turbulent-like regime, i.e., elastic turbulence, are still possible to occur in the limit of large enough Wi, under which Newtonian fluid flow is definitely in the laminar regime.[8–10] The occurrence of flow instability or turbulence without nonlinear inertia implies great potential in enhancing heat and mass transfer efficiency in the micro-scale areas,[11–15] as well as special functional design in microfluidics.[16,17]

The present paper focuses on the elastic turbulence where the elastic nonlinearity dominates. It has been over ten years since the first report on elastic turbulence by Groisman and Steinberg.[9] So far, numerous researches on this phenomenon have been carried out to obtain insight into its underlying mechanism as well as to realize its application. From the experimental viewpoint, most of the early work was limited to the geometry with local curvature such as the swirling flow between two parallel disks, Taylor–Couette flows between two coaxial cylinders, as well as micro-scale flows in the curvilin-

*Project supported by the National Natural Science Foundation of China (Grant Nos. 51276046 and 51506037), the Foundation for Innovative Research Groups of the National Natural Science Foundation of China (Grant No. 51421063), the China Postdoctoral Science Foundation (Grant No. 2016M591526), the Heilongjiang Postdoctoral Fund, China (Grant No. LBH-Z15063), and the China Postdoctoral International Exchange Program.

†Corresponding author. E-mail: lixb@hit.edu.cn
‡Corresponding author. E-mail: caiwh@hit.edu.cn

© 2016 Chinese Physical Society and IOP Publishing Ltd

ear micro-channels.[18,19] Therein, the elastic turbulence was described as the flow regime after elastic instability, with significant growth of drag resistance, a wide range of energy spectrum, and fluctuating vortex structures random in time but smooth in space, and so on. However, for a long time, the curvature of the geometrical configuration was considered to be indispensable for the flow transition from laminar to purely elastic instability according to the linear stability analysis.[20,21] In these cases, the existence of curvature induces "hoop stress", which is defined as the ratio of the local first normal stress difference and local curvature, and is responsible for the flow transition. McKinley[21] summarized the results in different geometries and put forward the critical condition for purely elastic instability: $\lambda U N_1/(R\Sigma) \geq M$, where M is a constant and related with the geometry, R is the streamline curvature, N_1 is the first normal stress difference, and Σ is the shear stress. In this condition, purely elastic instability and further elastic turbulence are considered to be impossible in a straight pipe or a parallel plate channel, since therein R is infinite, and the microstructures will be degraded before satisfying the above condition. However, the nonexistence of a linear transition does not guarantee the flow is absolutely stable, since only infinitesimal perturbations are taken into account in linear stability analysis. Actually, the finite perturbation usually exists in the real flow, where linear stability analysis loses its validity. The recent nonlinear stability analysis pointed out that the nonlinear transition is possible for inertialess viscoelastic flow.[22–24] It was then confirmed experimentally by Bonn[25] in a straight pipe and Pan[26] in a straight channel, where large fluctuations were firstly excited before entering measuring sections. In this straight pipe, it was found that the power law exponent of the energy spectrum is around -1.5, whereas it is between -3 and -4 in the curved geometry.[25]

As mentioned above, the elastic turbulence is induced by elastic nonlinearity. Therefore, knowledge of the microstructure characteristics is of primary importance to understand its underlying physical mechanism. Chu's group has carried out a series of experimental measurements of single polymer behaviors in elongational and shear flows,[27,28] where the coil-stretch transition of single polymer was reported. It has now been argued that the occurrence of microstructure coil-stretch transition is a prior for elastic turbulence.[29–31] Nevertheless, with the current experimental technique, it is quite difficult to directly measure microstructure behaviors or its role in the elastic turbulence except through indirect estimation such as the Lyapunov exponent or total drag resistance.[31–33] This strongly limits our understanding of the whole process of elastic turbulence from the experimental viewpoint. In this sense, direct numerical simulation has been proven to be a complement to the experimental approach for any turbulent flow for many years. Through directly solving the governing equations of viscoelastic flow, the detailed information including not only flow field but also microstructure conformation field could be achieved, which is so far impossible for experimental approaches. In fact, several numerical simulations have been carried out on elastic turbulence, such as the Taylor–Couette flow,[35,36] the Kolmogorov flow,[37–39] and the Stokesian flow,[40] the flow in a three-dimensional (3D) curvilinear channel,[41] and straight channel[42] of viscoelastic fluids, based on which our knowledge of elastic turbulence has been greatly enriched. Therein, similar characteristics to those in experiments were reproduced such as the significant increase of drag resistance, faster spectrum decay, and so forth. Moreover, except geometries with local curvature DNSs[37,39,42] have already been reported and confirmed before the experimental proof in Refs. [25] and [26] that the elastic instability and turbulence are possible to be excited even with only rectilinear streamline flow.

In spite of its great fascination to researchers and the extensive range of potential applications, the understating of the elastic turbulence is still quite limited by now, especially the elastic turbulence in the rectilinear shear flow. Following our previous work, the current work further discusses the characteristics of elastic turbulence including statistical properties and structural properties, as well as its maintenance from the viewpoint of the global energy budget. The paper is organized as follows: Section 2 introduces the numerical models and governing equations used in the following sections; the numerical results are then discussed in detail in Section 3; Section 4 draws the conclusion of the present paper.

2. Numerical model and basic equations

Direct numerical simulations (DNSs) of the viscoelastic fluid flow were carried out in a 3D parallel plate channel as illustrated in Fig. 1(a). As shown in Fig. 1(a), x, y, and z represent the streamwise, wall-normal, and spanwise directions, with the lengths of $10h$, $2h$, and $5h$, respectively. Here, h is the half height of the channel and u, v, w are the corresponding velocity components in each direction. The description of the viscoelastic fluid was expressed by the well-known Giesekus model. An additional sinusoidal force $\boldsymbol{F}$ ($\boldsymbol{F} = (F_{\mathrm{m}} \sin(2\pi y/h), 0, 0)$, with F_{m} the amplitude of the additional force, was exerted on the flow to generate a strong rectilinear shear inside the channel and sustain the turbulent motion from the viscous and elastic dissipation. According to the additional force $\boldsymbol{F}$, the flow could be divided into 4 layers for convenience of the following analysis, as shown in Fig. 1(b). The governing equations are as follows:

$$\frac{\partial u_i}{\partial x_i} = 0, \tag{1}$$

$$\frac{\partial u_i}{\partial t}+u_j\frac{\partial u_i}{\partial x_j}=-\frac{\partial p}{\partial x_i}+\frac{1}{Re}\frac{\partial^2 u_i}{\partial x_j\partial x_j}+\frac{\beta}{ReWi}\frac{\partial\left(C_{ij}-\delta_{ij}\right)}{\partial x_j}+f_i^*, \tag{2}$$

$$\frac{\partial C_{ij}}{\partial t}+u_k\frac{\partial C_{ij}}{\partial x_k}=C_{ik}\frac{\partial u_j}{\partial x_k}+C_{kj}\frac{\partial u_i}{\partial x_k}-\frac{\left[\delta_{ik}+\alpha\left(C_{ik}-\delta_{ik}\right)\right]\left(C_{kj}-\delta_{kj}\right)}{Wi}, \tag{3}$$

where the subscript i (i, $j=1,2,3$, respectively, corresponding to x, y, z directions) satisfies the summation convention; h is the imaginary laminar velocity amplitude $u_\mathrm{l}(u_\mathrm{l}=F_\mathrm{m}h^2/(4\pi 2\eta_\mathrm{s}))$ under the given additional force, h/u_l and ρu_l^2 are chosen as scales for length, velocity, time, and stress, respectively; η_s is the solvent contribution to the viscosity; β is the ratio of kinetic viscosity contributed by the solute (η_P) to the solvent contribution (η_s) and set to be 0.5 in all the following cases; $\boldsymbol{C}$ is the dimensionless conformation tensor of the viscoelastic solutions normalized by η_P; $\boldsymbol{I}$ is the unit tensor; α is the mobility factor of the Giesekus constitutive model and set to be 0.001 in all the following cases; Re and Wi are then defined as $Re=2u_\mathrm{l}h/(\eta_\mathrm{P}+\eta_\mathrm{s})$, $Wi=2\lambda u_\mathrm{l}/h$, respectively; λ is the relaxation time of viscoelastic fluid; and f_i^* is the dimensionless additional force, $\boldsymbol{f}^*=[2\pi\beta\sin(2\pi y)/Re,0,0]^\mathrm{T}$.

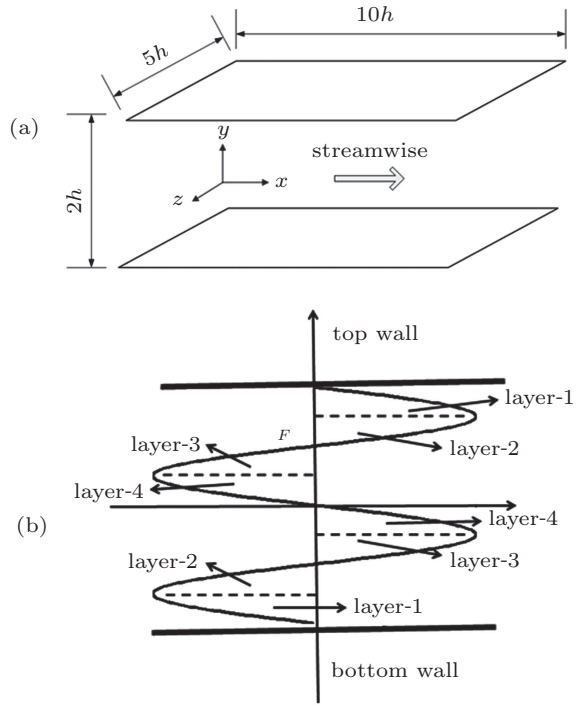


Fig. 1. Schematics diagram of (a) the simulated flow geometry and (b) form of the additional force $\boldsymbol{F}$. Here, to show the straight wall effect the flow is divided into 4 layers according to the form of the additional force.

As for the spatial discretization, a second-order central difference scheme is used for the momentum transport equation, while the MINMOD scheme is used for the convective term in the Giesekus constitutive equation. The Adams–Bashforth scheme is used for time advancing to keep a second-order accuracy in time. As for the boundary condition, periodic conditions are adopted for both streamwise and spanwise directions, and the non-slip boundary condition for the top and bottom walls. Moreover, Re is set to be 1 for all cases and the channel flow of Newtonian fluid is definitely laminar. The simulations are conducted in a mesh with $64\times64\times64$ grids, which has been verified to be fine enough for capturing all information desired for a very-low-Re elastic turbulence and is suitable for the computing resource in Ref. [42]. The further details on the numerical procedures could be found in Refs. [42] and [43].

For the convenience of later analysis, some basic variables are defined as follows. Based on the instantaneous velocity fields and polymer conformation, the global kinetic energy E_K, elastic energy E_p, the enstrophy W, and strain S are defined as follows:

$$\begin{aligned}E_\mathrm{K}&=\frac{1}{V}\iiint\frac{u_iu_i}{2}\mathrm{d}x\mathrm{d}y\mathrm{d}z,\\ E_\mathrm{p}&=\frac{1}{V}\iiint\frac{1-\beta}{Wi}(C_{xx}+C_{yy}+C_{zz})\mathrm{d}x\mathrm{d}y\mathrm{d}z,\\ W&=\frac{1}{V}\iiint\frac{\omega_i\omega_i}{2}\mathrm{d}x\mathrm{d}y\mathrm{d}z,\\ S&=\frac{1}{V}\iiint\frac{s_{ij}s_{ij}}{2}\mathrm{d}x\mathrm{d}y\mathrm{d}z,\end{aligned} \tag{4}$$

where V is the volume of the simulated geometry; ω_i is the instantaneous vorticity field: $\omega_i=(\partial u_\mathrm{k}/\partial x_j)\varepsilon_{ijk}$; s_{ij} is the strain tensor: $s_{ij}=(\partial u_i/\partial x_j+\partial u_i/\partial x_j)/2$.

For the turbulent cases, the instantaneous velocity u_i and polymer conformation field C_{ij} can be divided into the mean flow and the fluctuations i.e., $u_i=\langle u_i\rangle+u_i'$, and $C_{ij}=\langle C_{ij}\rangle+C_{ij}'$, where $\langle\cdot\rangle$ is the spatial temporal average over the streamwsie and spanwise plane (periodic in both directions) and varies in the normal direction y,

$$\langle f\rangle=\frac{1}{TS_xS_z}\int_0^T\iint f\mathrm{d}x\mathrm{d}z\mathrm{d}t.$$

Similarly, the global turbulent kinetic energy E_KF, turbulent enstrophy W_KF, and turbulent strain S_KF are defined as follows based on the fluctuating velocity and microstructure conformation fields:

$$\begin{aligned}E_\mathrm{KF}&=\frac{1}{V}\iiint\frac{u_i'u_i'}{2}\mathrm{d}x\mathrm{d}y\mathrm{d}z,\\ W_\mathrm{KF}&=\frac{1}{V}\iiint\frac{\omega_i'\omega_i'}{2}\mathrm{d}x\mathrm{d}y\mathrm{d}z,\\ S_\mathrm{KF}&=\frac{1}{V}\iiint\frac{s_{ij}'s_{ij}'}{2}\mathrm{d}x\mathrm{d}y\mathrm{d}z,\end{aligned} \tag{5}$$

where ω_i' and s_{ij}' are the fluctuating vorticity field and strain tensor based on the velocity fluctuations, respectively.

3. Results and analysis

To obtain further insight into this intriguing phenomenon, this section analyzes the numerical results focusing on the

structural and statistical characteristics, the generation and maintenance of the elastic turbulence following our previous study.[42] In our previous work, the critical criterion for the onset of elastic instability has been determined to be $Wi_c > 5$ under the same type of additional force. The following analysis is carried out mainly on the basis of the numerical databases, which have been proved to be above the onset of elastic instability in Ref. [42].

3.1. Characteristics of elastic turbulence

3.1.1. Flow patterns

We start our analysis on flow structures by considering the pattern of velocity field ($\boldsymbol{u} = [u, v, w]^{\mathrm{T}}$), polymers conformation field ($\boldsymbol{C}$) and the coherent structures in the rectilinear viscoelastic fluid flow when the elastic instability has been induced. Above the onset of the elastic instability, the flow experienced several stages by firstly to the quasi-periodically state, and then to a further irregular and disordered state with the elastic nonlinearity increasing. The discovery of coherent structures has significantly promoted the understanding of inertial turbulence, and abundant research has been paid to its detecting method, characteristics, generation mechanism, and so forth. In elastic turbulence, the coherent structures were also detected in Ref. [38] and appeared in the form of "elastic waves". So far, the understanding of coherent structures in elastic turbulence is however still in an initial stage due to the short research history of elastic turbulence and lack of a database. According to the definition in inertial turbulence, coherent structures can be roughly separated into two groups which are tube-like vortex structures (i.e., regions dominated by the rotating motion) and the sheet-like vortex structures (i.e., regions dominated by the deforming motion). Based on the velocity gradient tensor, several methods have now been proposed to identify the tube-like vortex structures. Herein, the coherent structures in viscoelastic fluid flow above the onset of elastic instability were also studied by investigating the vortex tube-like structures using the Q criterion.[44] The Q is the second invariant of the velocity-gradient tensor $\nabla \boldsymbol{u}$, and can be calculated by $Q = w_{ij}w_{ij} - s_{ij}s_{ij}$ where $w_{ij} = (\partial u_i/\partial x_j - \partial u_j/\partial x_i)/2$.

To have an intuitive impression of the flow structures in the viscoelastic fluid flow above elastic instability, firstly the snapshots of the velocity field $\boldsymbol{u}$, vortex tube-like structures Q, and microstructures extension $\mathrm{tr}(\boldsymbol{C})$ are presented in both the streamwise–normalwise (x–y) section and the streamwise–spanwise (x–z) section at the same time as shown in Figs. 2–4, respectively. From Fig. 2(a), the base flow of velocity component u shows periodicity in the normalwise section due to additional cosine force and breaks along the streamwise. The transversal component v shows some localized quadrupolar flow patterns of positive and negative values on the background of zero velocity, as found in Ref. [38]. In this manner, the localized vortex structures with scale on the order of the channel width are then formed. Around these flow patterns, as shown in Figs. 2(c) and 2(d), the strong tube-like structures with $Q > 0$ and sheet-like structures with $Q<0$ are embedded close to each other. Besides, as for the microstructures elongation, it shows disordered filament-like structures as shown in Fig. 2(b).

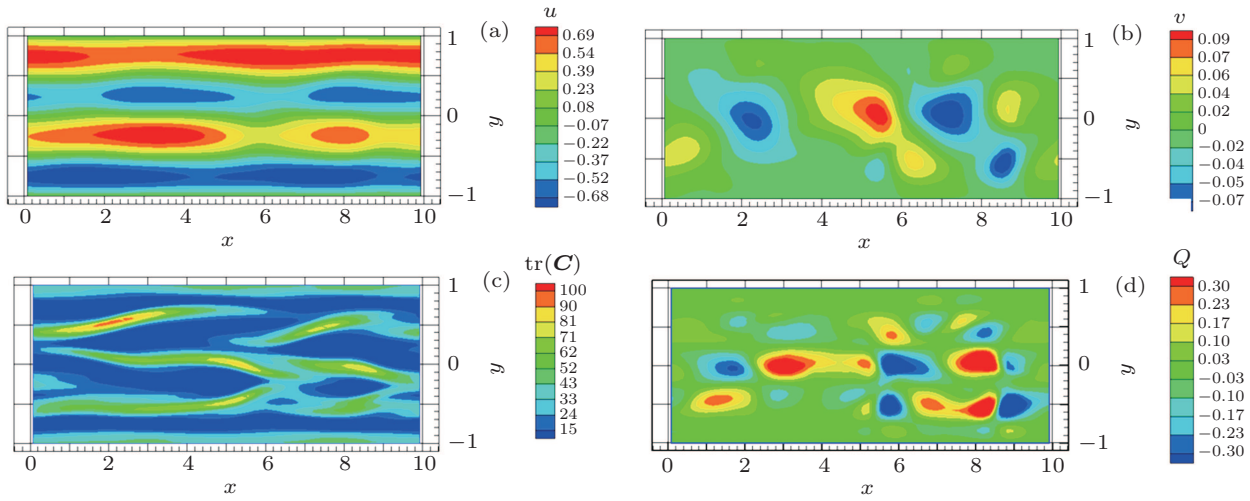


Fig. 2. (color online) Snapshots of different fields in the x–y section $z^* = S_z/2$ at the same time at $Wi = 30$: (a) u; (b) v; (c) $\mathrm{tr}(\boldsymbol{C}) = C_{xx} + C_{yy} + C_{zz}$; (d) Q.

In Refs. [37], [38], and [40], the elastic turbulence was numerically investigated in a 2D rectilinear shear flow and has reproduced some basic phenomenology observed in the experiments. However, for every turbulent flow, it should be definitely 3D. To improve our understanding on 3D properties of elastic turbulence, figures 3 and 4 present the characteristics of the flow motion in the streamwise–spanwise section. It indicates that with the increase of Wi, the further distorted

and irregular flow patterns could be formed along the spanwise with localized quadrupolar flow patterns similar to that in the streamwise. Correspondingly, the vortex tubes ($Q > 0$) are distorted in the spanwise, accompanied by the significantly deformed flow patterns ($Q < 0$), where polymers are strongly stretched as circled in Fig. 4. In other words, for the viscoelastic fluid flow above elastic instability vortex tube structures tend to be formed around the regions where the polymers are strongly stretched. With the increase of Wi, further disordered and random vortex tubes will be induced.

Moreover, the flow structures above elastic instability were also observed to be propagating along the streamwise with time in the form of elastic waves in the flow as reported in Ref. [38], which may be due to the non-homogeneous distribution of turbulent kinetic energy and polymer elastic potential energy. Figure 5 shows the spatial–temporal propagation of the flow and polymer structures at different Wi. It is obtained that the propagation firstly behaves regularly at $Wi = 10$ along the streamwise especially in the channel center where the vortex tubes and sheet appear alternatively. The propagating direction at different y is corresponding to the sign of local average velocity $u_{\mathrm{m}}(y)$ with the same propagating velocity $u_{\mathrm{p}}(u_{\mathrm{p}} = \Delta x/\Delta t$ where Δx is the propagating distance in the time interval $\Delta t)$ and flow patterns. Increasing Wi to above 20, the propagation became rather unstable and shaking along the streamwise direction. It then becomes difficult to determine u_{p} due to the unstable and interacting local flow motions. In addition, the close relation between the polymers elongation and the formation of the vortex tube structures could also be observed again by comparing Figs. 5(a) with 5(b), i.e., vortex tube structures tend to be formed in the regions where the microstructures were significantly stretched, in consistent with Fig. 4.

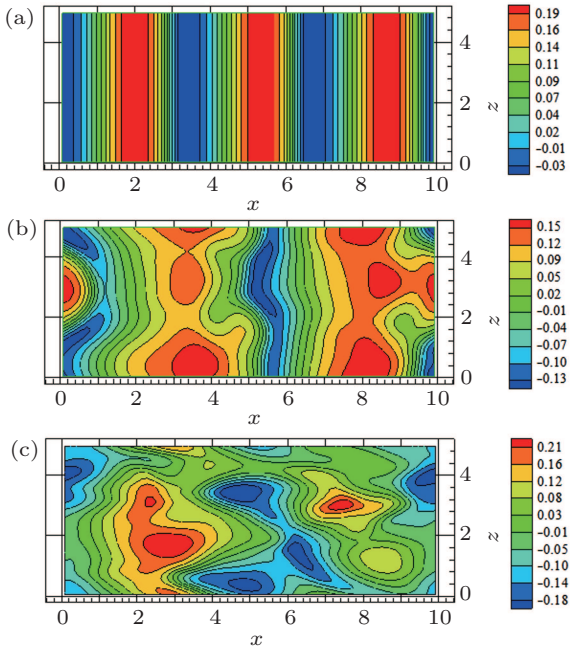


Fig. 3. (color online) Snapshots of flow motion (velocity component u) in the streamwise–spanwise (x–z) section $y^* = 0$ (with strong velocity gradient): (a) $Wi = 10$; (b) $Wi = 20$; (c) $Wi = 30$.

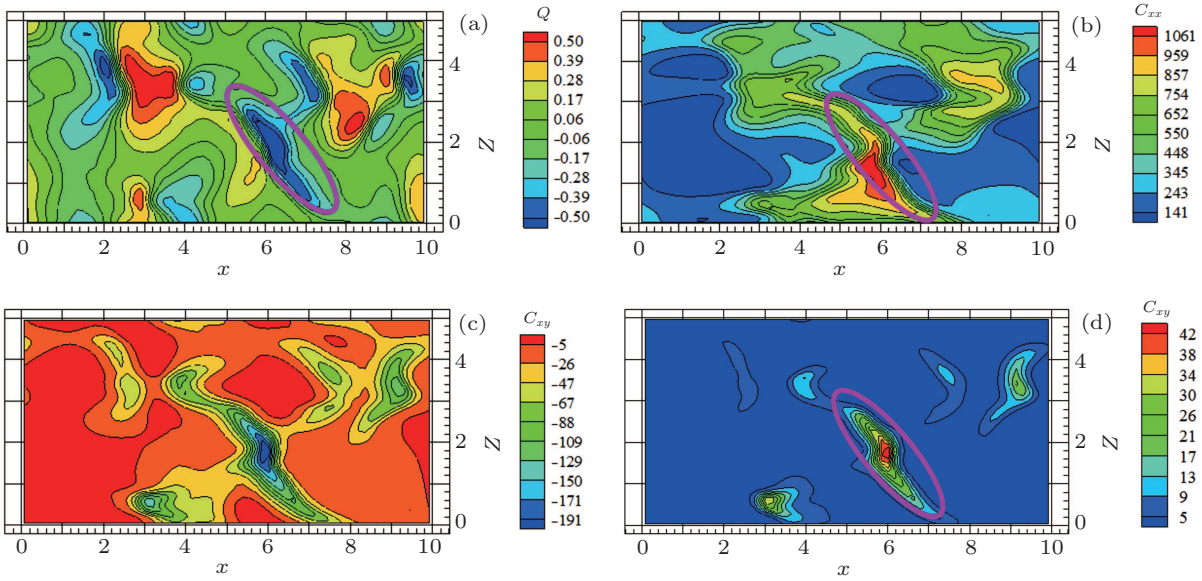


Fig. 4. (color online) The distribution and characteristics of vortex tubes and the polymer conformation components in the streamwise–spanwise (x–z) section $y^* = 0$ at $Wi = 30$: (a) Q; (b) C_{xx}; (c) C_{xy}; (d) C_{yy}.

3.1.2. Straight wall effect on elastic turbulence

In the present paper, the flow was divided into 4 layers according to additional force, so it is possible to study the straight wall effect on elastic turbulence by comparing flow characteristics in different layers. Before this comparison, we firstly compare the flow motion especially the turbulent statistics near the wall in this channel with that in the curvilinear channel, which could be found in our previous numerical

results obtained in a curvilinear channel[41] and this straight channel.[42] Similar to that in inertial turbulence and experimental observation in the curved geometry, two peaks of the velocity fluctuations could be observed near the wall for the curvilinear channel. However, in the current case, no peak of the velocity fluctuations is formed in layer-1, which is directly affected by the wall, indicating the straight wall may suppress the turbulent motion. In order to further confirm this, the attentions are then paid to the distributions of the microstructures extension and vortex structures as shown in Figs. 2 and 5(d), as well as the energy spectrum in different layers as shown in Fig. 6. As shown in Figs. 2 and 5(d), it could be found that the turbulent motion and strength are much stronger and quite similar from layer-2 to layer-4; only in the near wall region, though the microstructures are strongly stretched, the turbulence motions are significantly suppressed. In the layers far from the straight wall, $E(k)$ exhibits a power law decay with the exponent of -3.8, which is in consistent with the experimental observations in Refs. [9], [18], and [19] and the numerical data in Refs. [37] and [38]. However, in the layer next to the straight wall, though with significant velocity gradient, the turbulent kinetic energy shows a faster decay as shown in Fig. 6(a), which indicates that the elastic turbulence is locally suppressed by the straight wall. This is different from the role of the curvilinear wall in the elastic turbulence, which is regarded as the source of the elastic turbulence generation and near which the turbulent intensity is stronger.[19,41] It implies that in the real rectilinear shear flow the elastic turbulence is able to sustain by generating the strong shear in the center far from the wall, but the straight wall will suppress the elastic turbulence.

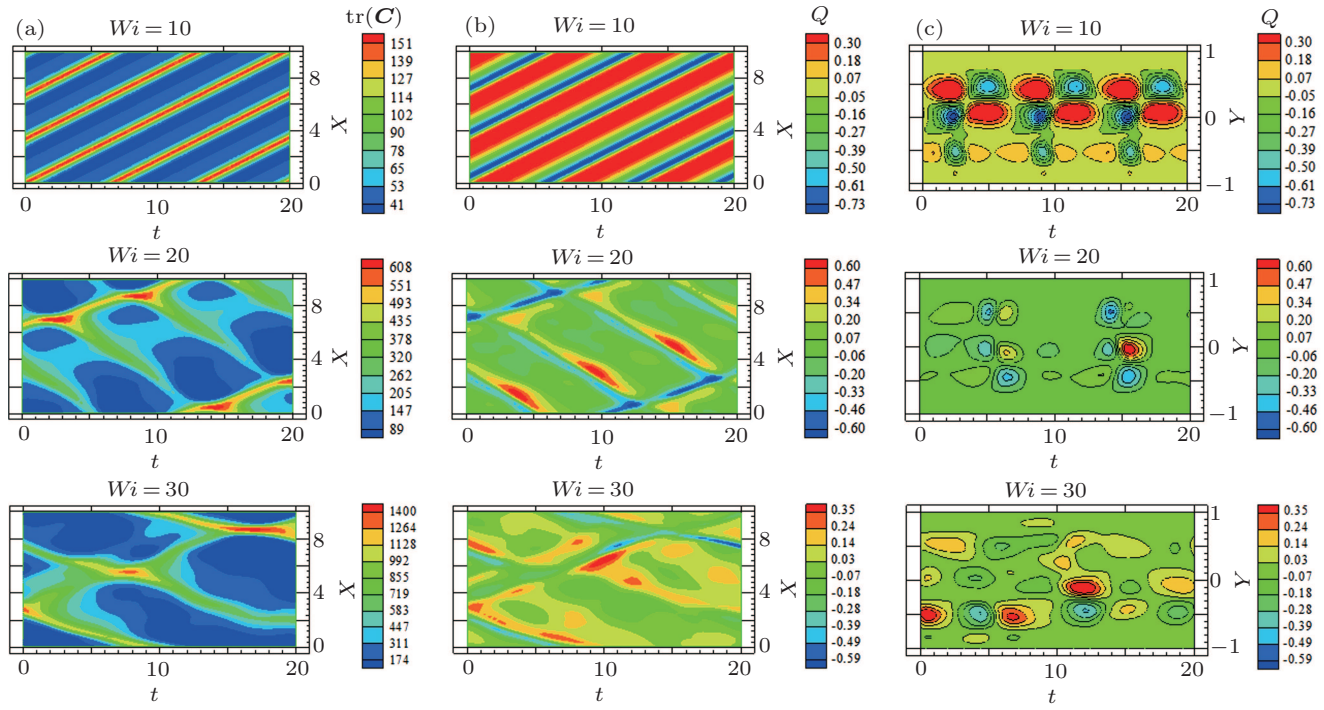


Fig. 5. (color online) Spatial–temporal propagation of the flow and polymer structures with the increase of *Wi*: (a) tr($\boldsymbol{C}$) along the streamwise at $y = 0$, $z = S_z/2$; (b) Q along the streamwise at $y = 0$, $z = S_z/2$; (c) Q along the normalwise at $x = S_x/2$, $z = S_z/2$.

It then becomes natural to ask why the straight wall suppresses the elastic instability and turbulence and then why it could survive in the current simulation even with a straight wall. The "hoop stress" theory is used here to answer the above question. According to our numerical study, even without the geometry curvature the viscoelastic fluid flow could still be elastically turbulent. It is conjectured that the key of elastic turbulence occurrence does not lie in the geometrical curvature but the streamline curvature. In the curvilinear channel, the geometry provides the curved streamline which generates the "hoop stress". The "hoop stress" then leads to the normal flow motion and amplifies the initial perturbations. In the current geometry, in the bulk flow region, the initial perturbations bring in the curved streamline by which the "hoop stress" could be generated and then maintain the elastic turbulence. Next to the wall, the flat-straight wall straightens the initial curved streamline, and then eliminates the "hoop stress". Therefore, the flow therein tends to be more stable. The straight wall suppression effect may not only exist in the low-*Re* flows but also high-*Re* flows. However, the affecting region is related with *Re*. For the large-*Re* flows such as inertial turbulent flows, its effect is mainly confined in a very thin

layer next to the wall, or within the thickness of the viscous sub-layer. Unlike large-*Re* flows, in the elastic turbulent flow with an extremely low *Re*, the straight wall effect will dominate the whole area if without any additional treatment. Then if the straight wall suppresses the elastic turbulent motion, why and how could it survive in the center? To answer this, the form of our external force and the role of layer-1 are considered. The existence of layer-1 (or the stable layer next to the wall) may block the straight wall effect from transferring into the center region. In this way the curved streamlines could be kept there far from the near wall region. In other words, this stable or blocking layer is of importance to the generation and maintenance of elastic turbulence in the channel without curvature. This conjecture still needs future experimental and numerical verifications.

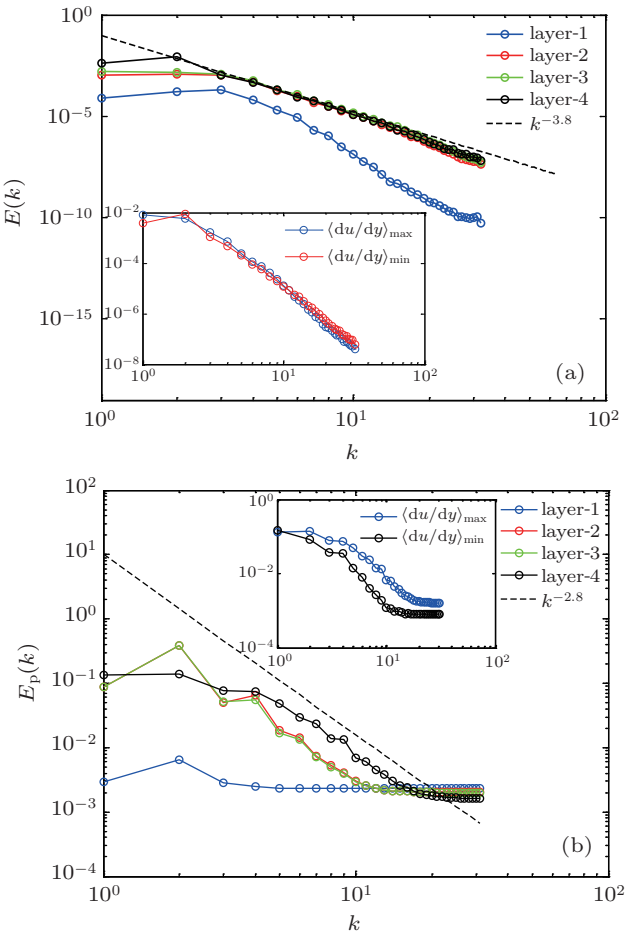


Fig. 6. (color online) Spectrums of (a) velocity fluctuations and (b) polymers extension in four layers with maximum local velocity gradient at $Wi = 30$. The inset shows the velocity gradient effect on the spectrums in layer-2. Following the definition of energy spectrum $E(k)$, $E_p(k)$ is defined as follows: $l_i = \sqrt{C_{ii}}$, $L_i(k) = \mathrm{FFT}(l_i)$ $(i = 1,2,3)$, $E_p(k) = [(1-\beta)/Wi]L_i(k)L_i^*(k)$. Here, $L_i^*(k)$ is the conjugate of $L_i(k)$.

Moreover, as shown in the inside inset of Fig. 6, the local mean velocity gradient has little effect on $E(k)$ in the layers away from the wall, except modifying the amplitude in the largest scale, which is related with the local turbulent intensities. The decaying of the elastic energy $E_p(k)$, which describes the multi-scale property of the elastic structures, is also investigated as shown in Fig. 6(b). It is observed that in the regions (layer-2 to layer-4) where the flow behaves as turbulent status, it shows a power law decay with the decaying exponent of -2.8 (equal to $kE(k)$) in the range where $E(k)$ shows power law decay. Compared with $E(k)$, the local mean velocity gradient modifies the amplitude of $E_p(k)$ at all scales and the scales range of $E_p(k)$ is much narrower than that of $E(k)$

3.1.3. Relationship between microstructures behavior and flow motion

In this section, the statistical relationship between the microstructure behavior and the flow motion (turbulent characteristics) is investigated for the cases above elastic instability. As mentioned above, elastic turbulence is originated from the elastic nonlinearity of the viscoelastic fluid, which is closely related with the velocity gradient $\nabla \boldsymbol{u}$ rather than u. The microstructures are stretched through the local velocity gradient in the form of $\nabla \boldsymbol{u} \cdot \boldsymbol{C} + \boldsymbol{C} \cdot \nabla \boldsymbol{u}^{\mathrm{T}}$. Therefore, for the future modeling of elastic turbulence, it would be necessary to study the relationship between the microstructures conformation and local velocity gradient. Figure 7 shows the statistical polymer conformation components as a function of the averaged velocity gradient $|\langle \mathrm{d}u/\mathrm{d}y\rangle|$ at the same location. It could be found that $\mathrm{tr}(\boldsymbol{C})$ and $|\langle C_{xy}\rangle|$ increase with the local velocity gradient $|\langle \mathrm{d}u/\mathrm{d}y\rangle|$ in the form of nearly quadratic and linear function, respectively. In the present paper, since α was set to a very small value, we ignore its effect. If so, the microstructure conformation $|\langle C_{xy}\rangle|$ will be linearly increased with both Wi and the local velocity gradient $|\langle \mathrm{d}u/\mathrm{d}y\rangle|$ in the laminar status, i.e., $|\langle C_{xy}\rangle|/|\langle \mathrm{d}u/\mathrm{d}y\rangle|$ linearly increases with Wi. As shown in Fig. 7(b), when the flow is above the elastic instability, it increases much faster than the predicted linear relationship, indicating the microstructures are above the coil-stretch transition. In addition, it is also found that $\langle C_{xx}\rangle \gg \langle C_{yy}\rangle > \langle C_{zz}\rangle$ indicating that the main contribution of the polymer elongation is from C_{xx} in the streamwise direction due to the current numerical geometry (in consistent with that in Ref. [38]). However, different from that in Ref. [38], where it states $\langle C_{xx}\rangle \gg \langle C_{yy}\rangle \gg |\langle\langle C_{xy}\rangle\rangle|$, in our numerical simulation, $\langle C_{xx}\rangle > |\langle C_{xy}\rangle| > \langle C_{yy}\rangle$ is observed. The possible reason for the difference is as follows: in Ref. [29], $|\langle\langle C_{xy}\rangle\rangle|$ was obtained based on the average in the whole simulated geometry including the transversal direction, and should be closer to 0 due to the periodic condition in their simulation. Therefore, the relation $\langle C_{xy}\rangle \approx 10|\langle C_{xy}\rangle|$ in the flow above elastic instability in Ref. [38] is possibly only a coincidence and the transition of $|\langle C_{xy}\rangle|$ may be due to the lack of ensemble data during the averaging when the flow is above elastic instability. Moreover, when the flow is above elastic instability, as shown in Fig. 7(e), $|\langle C_{xx}\rangle|/|\langle C_{xy}\rangle|$ is observed to firstly decrease with the

local velocity gradient $|\langle \mathrm{d}u/\mathrm{d}y\rangle|$ and then gradually converge to a certain value, which increases with Wi. From Fig. 7(f), $|\langle C_{xx}\rangle|/|\langle C_{yy}\rangle|$ is observed to increase with Wi and the local velocity gradient $|\langle \mathrm{d}u/\mathrm{d}y\rangle|$ and could be much larger than 10, indicating that the increase of $|\langle C_{yy}\rangle|$ is slower than that of $|\langle C_{xx}\rangle|$. Moreover, it firstly shows a form of quadratic function and then slows down to a linear form due to the rising of $|\langle C_{yy}\rangle|$ in the location with a larger velocity gradient. Figure 8 shows the relationship between some turbulent statistics and the averaged velocity gradient at the same location. A strong relevance of the turbulent statistics on the local velocity gradient could be observed. All the fluctuations increase with velocity gradient and faster for the larger Wi. The turbulence intensities including both the flow motion and the polymer relaxation increase with the local velocity gradient, further confirming the domination of the velocity gradient in the elastic turbulence.

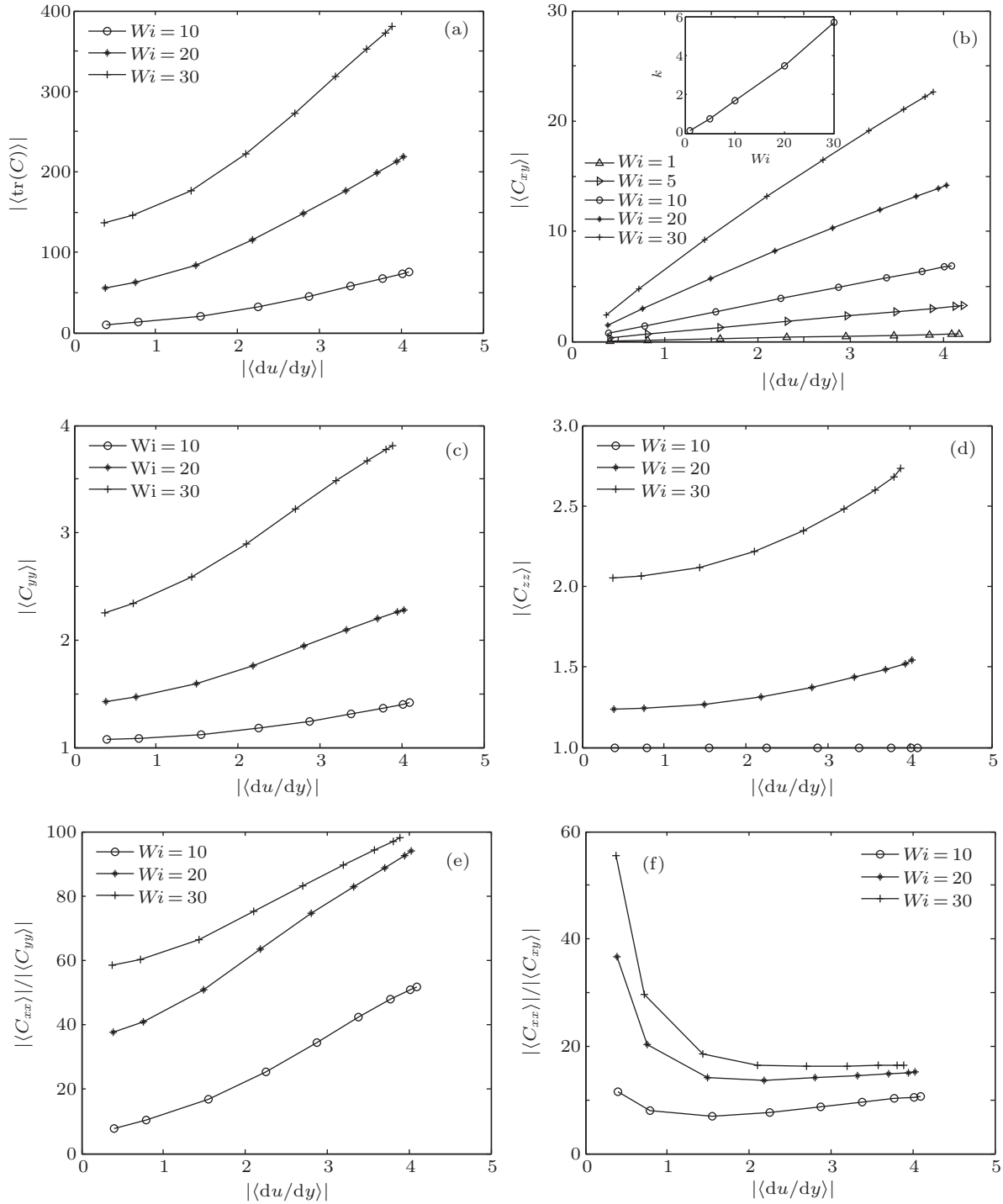


Fig. 7. Averaged local velocity gradient $|\langle \mathrm{d}u/\mathrm{d}y\rangle|$ at different Wi: (a) $|\langle \mathrm{tr}(\boldsymbol{C})\rangle|$; (b) $|\langle C_{xy}\rangle|$; (c) $|\langle C_{yy}\rangle|$; (d) $|\langle C_{zz}\rangle|$; (e) $|\langle C_{xx}\rangle|/|\langle C_{yy}\rangle|$; (f) $|\langle C_{xx}\rangle|/|\langle C_{xy}\rangle|$.

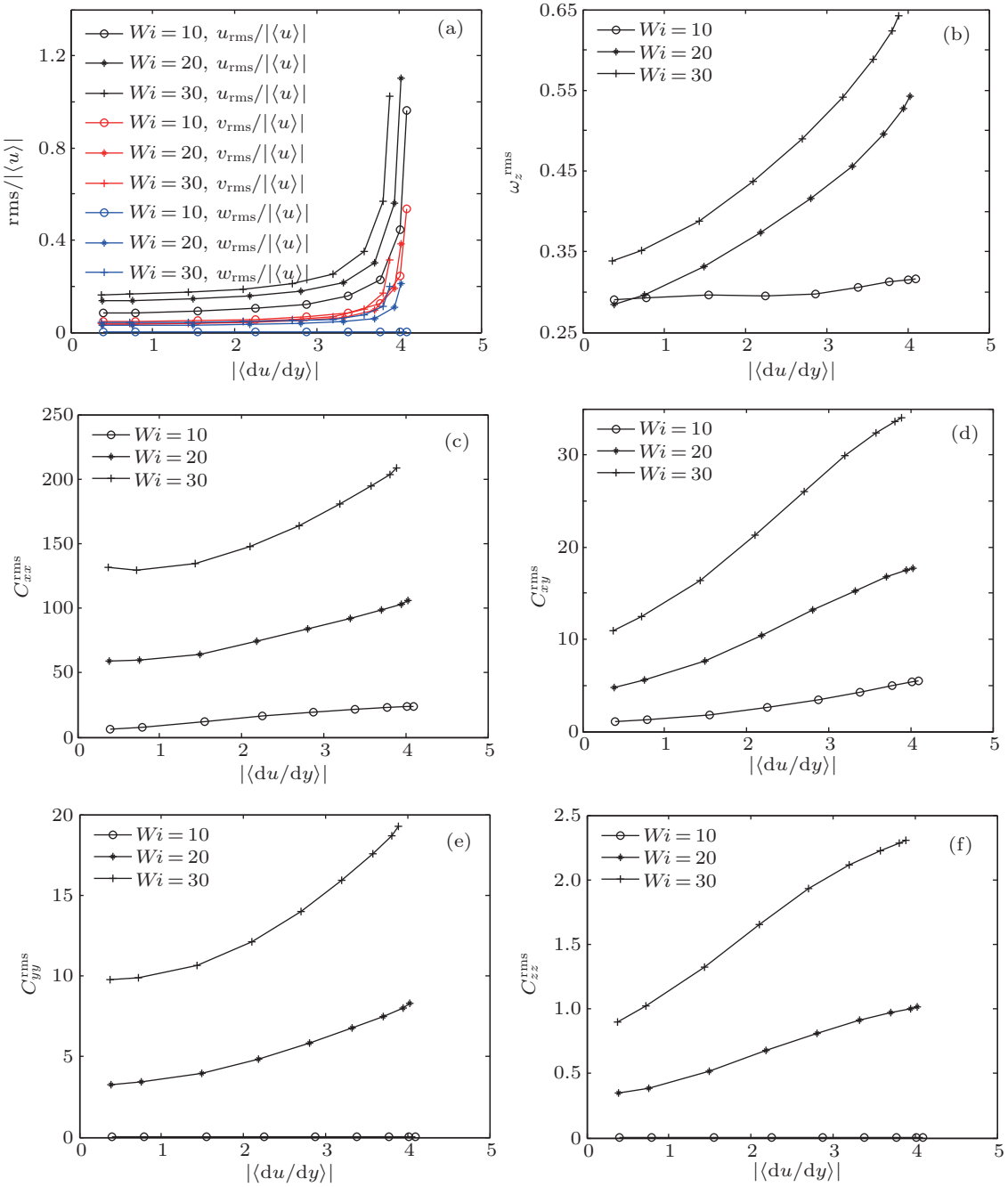


Fig. 8. (color online) Root mean square (rms) of velocity fluctuations and fluctuating polymerconformation components as a function of the averaged local velocity gradient at different *Wi*: (a) $u_{\rm rms}$, $v_{\rm rms}$, and $w_{\rm rms}$; (b) the rms of the vorticity, $\omega_z^{\rm rms}$; (c) $C_{xx}^{\rm rms}$; (d) $C_{xy}^{\rm rms}$; (e) $C_{yy}^{\rm rms}$; (f) $C_{zz}^{\rm rms}$.

3.2. Generation and maintenance of the elastic turbulence

In the inertial turbulence, the turbulent fluctuations and the vortex structures are generated and maintained through the Reynolds stress $\langle u_i' u_j' \rangle$, for which a series of theories and models have now been well established.[45] However, so far for the elastic turbulence which is dominated by the microstructures, there has been no detailed theory about its generation and maintenance. This section will discuss how the elastic turbulence is generated and sustained by mimicking the method used in inertial turbulence. Unlike Newtonian fluid, the microstructures embedded in the fluid are capable of storing energy during its stretching by main flow and also providing energy to the flow during its relaxation. Therefore, in the viscoelastic fluid flow, an infinite fluid element contains both the kinetic energy and elastic energy. The additional energy exchanges between the main flow and microstructures should be particularly taken into account. In the following, the generation and maintenance of turbulent energy and also vortex structures are studied by discussing the global budget from both instantaneous and fluctuating energetic viewpoints.

Before showing the numerical results, the energy budget for viscoelastic fluid flow was firstly derived. According to

Eqs. (2) and (3), it is easy to obtain the global balance for the instantaneous $E_{\rm K}$, fluctuating kinetic energy $E_{\rm KF}$, and elastic energy $E_{\rm p}$ as follows:

$$\frac{{\rm d}E_{\rm K}}{{\rm d}t} = -\varepsilon_{\rm v} - G_{\rm p} + F_{\rm K}, \tag{6}$$

$$\frac{{\rm d}E_{\rm KF}}{{\rm d}t} = P_{\rm K} - \varepsilon'_{\rm v} - G'_{\rm p}, \tag{7}$$

$$\frac{{\rm d}E_{\rm p}}{{\rm d}t} = \frac{{\rm d}E_{\rm p}}{{\rm d}C_{ii}}\frac{{\rm d}C_{ii}}{{\rm d}t} = G_{\rm p} - \varepsilon_{\rm p}, \tag{8}$$

where $F_{\rm K}$ is the energy input by the additional force; $G_{\rm p}$ is the energy exchange between the flow motion and polymers: $G_{\rm p} > 0$ indicating the energy is absorbed from the flow motion into the polymers, otherwise, the energy is released to the flow mainly from polymers; $\varepsilon_{\rm v}$ is the viscous dissipation of the kinetic energy; $\varepsilon_{\rm p}$ is the elastic dissipation; $P_{\rm K}$ is the energy exchange between the mean flow and the turbulent fluctuations by the Reynolds stress, and is regarded as the turbulent production term in the inertial turbulence with $P_{\rm K} > 0$; $\varepsilon'_{\rm v}$ is the viscous dissipation of the turbulent fluctuations; $G'_{\rm p}$ is the elastic effect on the turbulent fluctuations. The detailed expressions of each term can be found in Appendix A.

Firstly, the evolutions of $E_{\rm K}$, $E_{\rm p}$, and $E_{\rm KF}$ are shown in Fig. 9, showing that the flow achieves a statistically steady state with these three kinds of energy oscillating around certain values respectively. The temporal evolution oscillated stronger with an increase of Wi and the relative turbulent intensity increases to 5.2% at Wi =30. Moreover, from the evolution of $E_{\rm KF}$, it could be found that the flow behaves more intermittently and the flow structures with a large time scale are generated. As for the elastic energy $E_{\rm p}$, it shows a much larger time scale compared with the flow motion. Furthermore, figure 10 shows the kinetic energy balance (Eqs. (6) and (7)) from both instantaneous and fluctuating viewpoints at $Wi = 30$. From the instantaneous viewpoint, for the developed turbulent elastic turbulent flow, the energy balance is: ${\rm d}E_{\rm K}/{\rm d}t \approx 0$, and $F_{\rm K} \approx G_{\rm p} + \varepsilon_{\rm v}$, i.e., the additional force supplies and maintains the flow from viscous dissipation of the flow and the energy transfer to the microstructures. The energy transfer between the flow motion and microstructures $G_{\rm p}$ is positively oscillating, indicating the microstructures absorb energy from the main flow. This part of energy is then stored and dissipated by its relaxation during the evolution. With the increase of Wi, a more remarkable part of energy is transferred from flow structures to microstructures. Similarly, from the fluctuating viewpoint, the energy balance is: ${\rm d}E_{\rm KF}/{\rm d}t \approx 0$ and $P_{\rm R} - G_{\rm p} - \varepsilon_{\rm v} \approx 0$, for the developed turbulent flow without the additional power supply. As well known in inertial turbulence, $P_{\rm K} > 0$ and the Reynolds stress plays a dominated role in the turbulent kinetic energy production. However, it becomes incorrect for the elastic turbulence. As shown in Fig. 1(b), unlike that in the inertial turbulence, the production term $P_{\rm K}$ is close to 0 and thus can be ignored. The elastic term $G'_{\rm p}$, becomes dominated and positively skewed to counteract the viscous turbulent dissipation. In other words, it is the elastic term which keeps the turbulent fluctuations from vanishing.

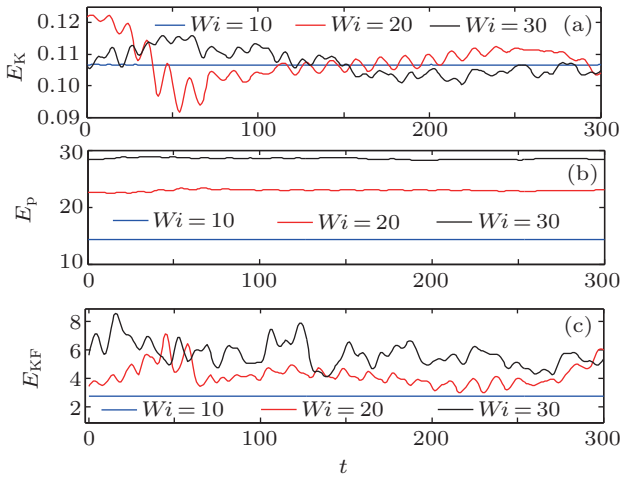


Fig. 9. (color online) Temporal evolution of the global quantities including $E_{\rm K}$ (a), $E_{\rm p}$ (b) and $E_{\rm KF}$ (c) at different Wi.

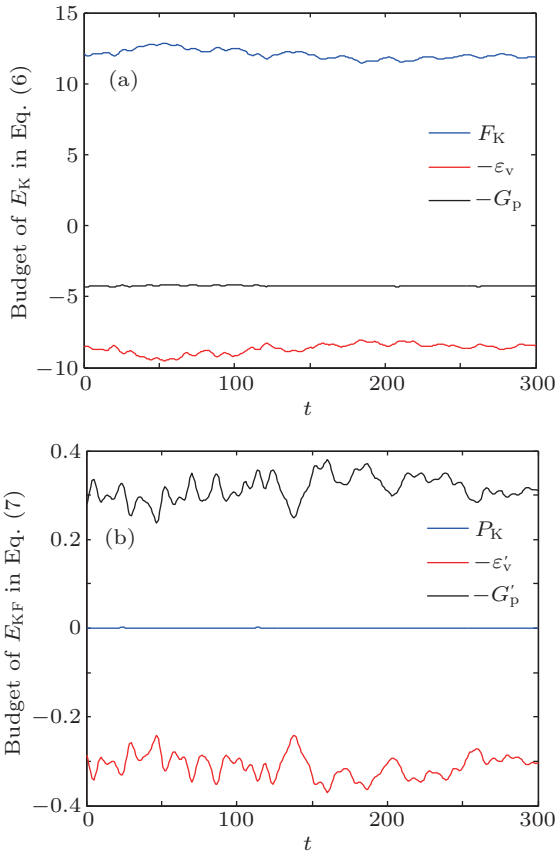


Fig. 10. (color online) Temporal evolution of kinetic energy budget at $Wi = 30$: (a) $E_{\rm K}$ based on Eq. (6) and (b) $E_{\rm KF}$ based on Eq. (7).

In order to further understand this process, the instantaneous and fluctuating elastic effect $G_{\rm p}$ and $G'_{\rm p}$ are focused. The above results mean that in the elastic turbulence, apparently the polymers are stretched by the main flow, i.e., C_{ij} and

$\partial u_i/\partial x_j$ are positively correlated, but if the fluctuations are considered C'_{ij} and $\partial u'_i/\partial x_j$ are negatively correlated, indicating that the flexibility of microstructures dominates the generation of the fluctuating velocity gradients. Therefore, unlike that in the inertial turbulence, $G'_{\rm p}$ is the energy production term in elastic turbulence. Note that enough energy should be released to support an elastic turbulence state due to the strong viscous dissipation at such a low Reynolds number. Therefore, we could attribute the generation and maintenance of the elastic turbulence to there being enough energy transfering from the microstructures into the flow during its relaxation.

Finally, the generation and maintenance of vortex structures are discussed. In inertial turbulence, relative to the velocity fields, the velocity gradient contains more significant fluid mechanical information and its dynamical behavior is closely related with the mechanism of vortex stretching and the energy cascade.[45] Therefore, it is of primary importance to investigate the generation of the velocity gradient in a turbulent flow to understand its kinematics and dynamics. As mentioned before, the characteristics of elastic turbulence are quite different from those of inertial turbulence, such as vortex structures comparable with the scale of the flow geometry and faster decay of the turbulent kinetic energy.[9] These differences may lie in the generation of velocity gradient, which is the focus of this part: investigating the energy budget of global enstrophy (indicating the strength of rotating motion in the flow) and strain (indicating the strength of deforming motion in the flow) as well as the microstructure effect therein.

The global budgets of enstrophy and strain from the instantaneous and fluctuating viewpoints are as follows:

$$\frac{{\rm d}W}{{\rm d}t} = W_{\rm R} - W_{\rm v} - W_{\rm p} + F_{\rm W}, \tag{9}$$

$$\frac{{\rm d}S}{{\rm d}t} = S_{\rm R} - S_{\rm v} - S_{\rm p} + F_{\rm S}, \tag{10}$$

$$\frac{{\rm d}W_{\rm KF}}{{\rm d}t} = P_{\rm W} - W'_{\rm v} - W'_{\rm p}, \tag{11}$$

$$\frac{{\rm d}S_{\rm KF}}{{\rm d}t} = P_{\rm S} - S'_{\rm v} - S'_{\rm p}, \tag{12}$$

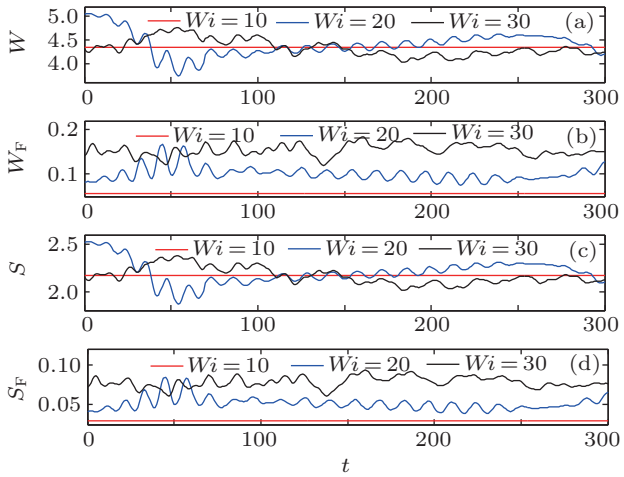


Fig. 11. (color online) Temporal evolution of the enstrophy and strain from instantaneous and fluctuating viewpoints at different Wi. (a) W, (b) $W_{\rm F}$, (c) S, (d) $S_{\rm F}$.

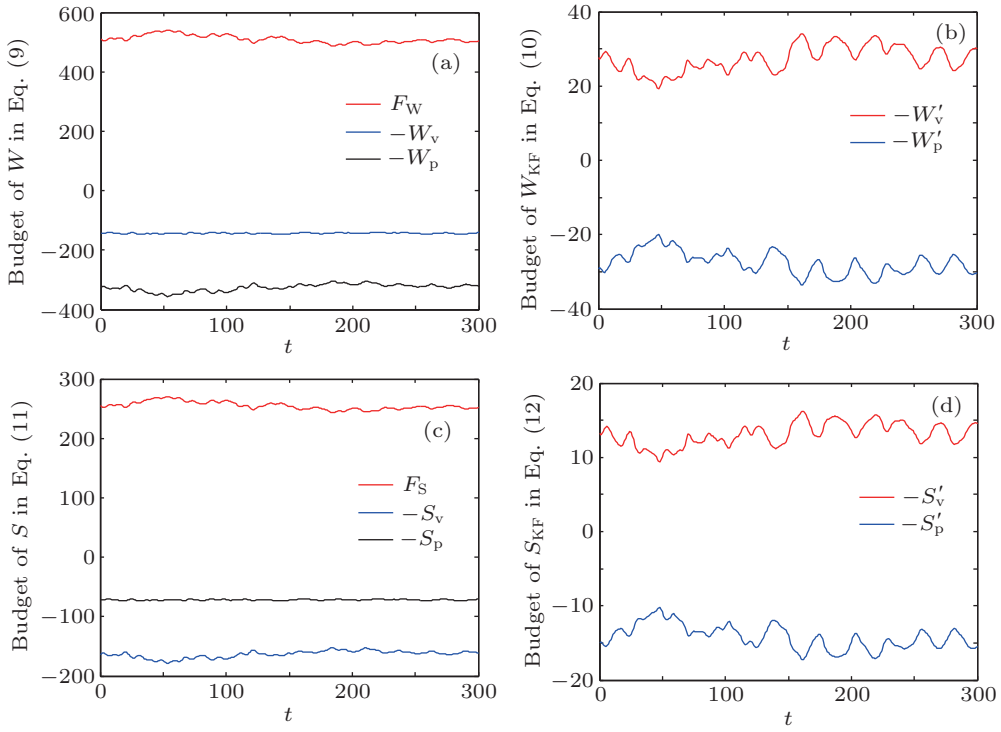


Fig. 12. (color online) Temporal evolution of budget for (a) W based on Eq. (9)); (b) $W_{\rm KF}$ based on Eq. (10); (c) S based on Eq. (11); and (d) $S_{\rm KF}$ based on Eq. (12) at $Wi = 30$.

where W_R is the vortex extension term by the velocity fields; W_v is the viscous effect of the global enstrophy; W_p is the elastic effect on the global enstrophy; F_W is the additional force effect on the global strain; S_R is the self-amplification of the strain and vortex extension effect on the generation of global strain; S_v is the viscous effect of the global strain; S_p is elastic effect on the global strain; F_S is the additional force effect on the global strain; P_W is the enstrophy exchange between the mean flow and turbulent flow structures, and also regarded as the production term for the inertial turbulence, with $P_W > 0$; W'_v is the viscous dissipation of turbulent enstrpohy; W'_p is the elastic effect on turbulent enstrophy; P_S is the strain exchange from the mean flow to the turbulent flow structures; S'_v is the viscous dissipation of the turbulent strain; S'_p is the elastic effect on the turbulent strain. The detailed expressions of each term can be found in Appendix A.

Figure 11 shows the evolutions of W, W_F, S, and S_F which are similar to those of E_K and E_{KF}, and the fluctuating enstrophy and strain are increasing with that of Wi. Figure 12 shows the evolutions of the budget of global enstrophy and strain from both the instantaneous and fluctuating viewpoints. From the instantaneous viewpoint, $F_W \approx W_p + W_v$ and $F_S \approx S_p + S_v$, i.e., the additional force maintains the enstrophy and strain by counteracting the viscous and elastic effect, and P_W and P_S can be ignored. From the fluctuating viewpoint, without the additional energy input, the fluctuating enstrophy and strain come from W'_p ($W'_p \approx -W'_v$) and S'_p($S'_p \approx -S'_v$), which are the interaction among the polymer conformation, the vorticity and strain. However, W'_R and S'_R (the vortex tube stretching and the strain self-amplification) which are dominant in the inertial turbulence can be ignored here. Therefore, in the elastic turbulence, it can be seen that the vortex tubes are mainly stretched by the polymers, and the strain and the polymer conformation in the flow are amplified by their interaction as compared with that in the inertial turbulence.

4. Conclusion

So far, the elastic turbulence is still poorly understood, due to the limitation of experimental techniques and the lack of numerical data, therefore our main goal is to obtain further insight to improve our knowledge of this intriguing phenomenon. DNSs of purely elastic turbulence in a 3D straight channel were carried out. Though the simulated geometry is very simple, most of the qualitative similar experimental observations have been reproduced in the current simulation. Following our previous research, the detailed characteristics of the elastic turbulence including the flow patterns and the role of velocity gradient, and the generation and maintenance from the energetic view point were presented in this paper. It is observed that in the elastic turbulence, the flow shows three dimensional characteristics with larger spatial scales, and the polymer elongation shows filament structures. The vortex tubes were found to be embedded in the regions where the polymers are strongly stretched. Besides, the straight wall effect on the characteristics was also investigated based on the kinetic energy and elastic energy spectrum, which indicates that the turbulent flow near the straight wall decays much faster, i.e., the straight wall tends to stabilize the turbulent flow. On the other hand, the existence of layer-1 in the simulation localizes this effect, which helps the fluctuations in the outer layers to survive from the straight wall effect. Moreover, in the elastic turbulent flow, the velocity gradient plays a dominant role in the flow characteristics, for example, the turbulent intensity is found to increase with that of the velocity gradient. As for the generation and maintenance of elastic turbulence, from the energetic viewpoint, it is found apparently from the instantaneous viewpoint that the additional force counteracts the viscous dissipation and elastic absorption, and the polymers absorb energy from the main flow. However, different from the inertial turbulence, there is continuous energy released from the polymers into the flow, which counteracts the viscous dissipation and sustains the turbulent status from the fluctuating viewpoint. Therefore, in elastic turbulence, we reach a conclusion that it is the fact that enough energy is released from the polymers which generates and maintains the elastic turbulence.

Appendix A

Expressions of the terms in Eqs. (6)–(12) are as follows:

$$\varepsilon_v = \frac{1}{V}\iiint \frac{\beta}{Re}\frac{\partial u_i}{\partial x_j}\frac{\partial u_i}{\partial x_j}\mathrm{d}x\mathrm{d}y\mathrm{d}z;$$

$$G_p = \frac{1}{V}\iiint \frac{1-\beta}{Wi}C_{ij}\frac{\partial u_i}{\partial x_j}\mathrm{d}x\mathrm{d}y\mathrm{d}z;$$

$$F_K = \frac{1}{V}\iiint f u_i \mathrm{d}x\mathrm{d}y\mathrm{d}z;$$

$$P_K = \frac{1}{V}\iiint u'_1 u'_2 \frac{\partial \langle u_1\rangle}{\partial x_2}\mathrm{d}x\mathrm{d}y\mathrm{d}z;$$

$$\varepsilon'_v = \frac{1}{V}\iiint \frac{\beta}{Re}\frac{\partial u'_i}{\partial x_j}\frac{\partial u'_i}{\partial x_j}\mathrm{d}x\mathrm{d}y\mathrm{d}z;$$

$$G'_p = \frac{1}{V}\iiint \frac{1-\beta}{Wi}C'_{ij}\frac{\partial u'_i}{\partial x_j}\mathrm{d}x\mathrm{d}y\mathrm{d}z;$$

$$W_R = \frac{1}{V}\iiint \omega_i\omega_j s_{ij}\mathrm{d}x\mathrm{d}y\mathrm{d}z;$$

$$W_v = \frac{1}{V}\iiint \frac{\beta}{Re}\frac{\partial \omega_i}{\partial x_j}\frac{\partial \omega_i}{\partial x_j}\mathrm{d}x\mathrm{d}y\mathrm{d}z;$$

$$W_p = \frac{1}{V}\iiint \frac{1-\beta}{Wi}\frac{\partial \omega_i}{\partial x_m}\frac{\partial C_{km}}{\partial x_j}\varepsilon_{ijk}\mathrm{d}x\mathrm{d}y\mathrm{d}z;$$

$$F_W = \frac{1}{V}\iiint \omega_i\frac{\partial f_k}{\partial x_j}\varepsilon_{ijk}\mathrm{d}x\mathrm{d}y\mathrm{d}z;$$

$$S_R = \frac{1}{V}\iiint [-s_{ik}s_{kj}s_{ij} - (\omega_i\omega_j s_{ij} - \omega_i\omega_i s_{ij}\delta_{ij})/4]\mathrm{d}x\mathrm{d}y\mathrm{d}z;$$

$$S_{\rm v}=\frac{1}{V}\iiint\frac{\beta}{Re}\frac{\partial s_{ij}}{\partial x_{\rm k}}\frac{\partial s_{ij}}{\partial x_{\rm k}}{\rm d}x{\rm d}y{\rm d}z;$$

$$S_{\rm P}=\frac{1}{V}\iiint\frac{1-\beta}{Wi}\frac{\partial s_{ij}}{2\partial x_{\rm k}}\left(\frac{\partial C_{ik}}{\partial x_{\rm k}}+\frac{\partial C_{jk}}{\partial x_i}\right){\rm d}x{\rm d}y{\rm d}z;$$

$$F_{\rm S}=\frac{1}{V}\iiint\frac{s_{ij}}{2}\left(\frac{\partial f_i}{\partial x_j}+\frac{\partial f_j}{\partial x_i}\right){\rm d}x{\rm d}y{\rm d}z;$$

$$P_{\rm W}=\frac{1}{V}\iiint\left(2\omega_1'\omega_2'\langle s_{12}\rangle+\omega_i's_{\rm i3}'\langle\omega_3\rangle+\omega_i'\omega_j's_{ij}'-\omega_3'u_2'\frac{\partial\langle\omega_3\rangle}{\partial x_2}\right){\rm d}x{\rm d}y{\rm d}z;$$

$$W_{\rm v}'=\frac{1}{V}\iiint\frac{\beta}{Re}\frac{\partial\omega_i'}{\partial x_j}\frac{\partial\omega_{\rm i}'}{\partial x_j}{\rm d}x{\rm d}y{\rm d}z{\rm d}x{\rm d}y{\rm d}z;$$

$$W_{\rm p}'=\frac{1}{V}\iiint\frac{1-\beta}{Wi}\frac{\partial\omega_i'}{\partial x_{\rm m}}\frac{\partial C_{\rm km}'}{\partial x_j}\varepsilon_{\rm ijk}{\rm d}x{\rm d}y{\rm d}z;$$

$$P_{\rm S}=\frac{1}{V}\iiint\left[-2\langle s_{12}\rangle s_{\rm 1}'{}_js'{}_{\rm 2}{}_{ji}-s_{ik}'s_{\rm kj}'s_{ij}'-u_2's_{12}'\frac{\partial\langle s_{12}\rangle}{\partial x_2}\right]{\rm d}x{\rm d}y{\rm d}z-\frac{1}{V}\iiint\frac{1}{4}\left(2\omega_i's_{\rm i3}'\langle\omega_3\rangle-2\omega_3's_{ij}'\langle\omega_3\rangle\delta_{ij}+\omega_i'\omega_j's_{ij}'-\omega_i'\omega_j's_{ij}'\delta_{ij}\right){\rm d}x{\rm d}y{\rm d}z;$$

$$S_{\rm v}'=\frac{1}{V}\iiint\frac{\beta}{Re}\frac{\partial s_{ij}'}{\partial x_j}\frac{\partial s_{ij}'}{\partial x_j}{\rm d}x{\rm d}y{\rm d}z{\rm d}x{\rm d}y{\rm d}z;$$

$$S_{\rm p}'=\frac{1}{V}\iiint\frac{1-\beta}{Wi}\frac{\partial s_{ij}'}{2\partial x_{\rm k}}\left(\frac{\partial C_{ik}'}{\partial x_{\rm k}}+\frac{\partial C_{jk}'}{\partial x_i}\right){\rm d}x{\rm d}y{\rm d}z.$$

References

[1] Bird R B, Curtiss C F, Armstrong R C and Hassager O 1987 *Dynamics of Polymers Liquids* (New York: Wiley)
[2] Toms B A 1949 *Proc. 1st Int. Congr. Rheol.* (North Holland)
[3] Sreenivasan K R and White C M 2000 *J. Fluid Mech.* **409** 149
[4] Shao X M, Lin J Z, Wu T and Wu Y L 2002 *Canadian J. Chem. Eng.* **80** 293
[5] Li F C, Kawaguchi Y, Segawa T and Hishida K 2004 *Phys. Fluids* **16** 3281
[6] Li F C, Kawaguchi Y, Segawa T and Hishida K 2005 *Phys. Fluids* **17** 075104
[7] Cai W H, Li F C and Zhang H N 2010 *J. Fluid Mech.* **665** 334
[8] Shaqfeh E S G 1996 *Annu. Rev. Fluid Mech.* **28** 129
[9] Groisman A and Steinberg V 2000 *Nature* **405** 53
[10] Li F C, Kinoshita H, Li X B, Oishi M, Fujii T and Oshima M 2010 *Exp. Thermal Fluid Sci.* **34** 20
[11] Groisman A and Steinberg V 2001 *Nature* **410** 905
[12] Burghelea T, Segre E and Steinberg V 2004 *Phys. Rev. Lett.* **92** 164501
[13] Burghelea T, Segre E, Bar-Joseph I, Groisman A and Steinberg V 2004 *Phys. Rev. E* **69** 066305
[14] Whalley R D, Abed W M, Dennis D J C and Poole R J 2015 *Theor. Appl. Mech. Lett.* **5** 103
[15] Whalley R D, Abed W M, Dennis D J C and Poole R J 2015 *Theor. Appl. Mech. Lett.* **5** 103
[16] Groisman A, Enzelberger M and Quake S R 2003 *Science* **300** 955
[17] Groisman A and Quake S R 2004 *Phys. Rev. Lett.* **92** 094501
[18] Groisman A and Steinberg V 2004 *New J. Phys.* **6** 29
[19] Burghelea T, Segre E and Steinberg V 2007 *Phys. Fluids* **19** 053104
[20] Pakdel P and McKinley G H 1996 *Phys. Rev. Lett.* **77** 2459
[21] McKinley G H, Pakdel P and Oztekin A 1996 *J. Non-Newtonian Fluid Mech.* **67** 19
[22] Morozov A and van Saarloos W 2005 *Phys. Rev. Lett.* **95** 024501
[23] Hoda N, Jovanović M R and Kumar S 2008 *J. Fluid Mech.* **601** 407
[24] Jovanović M R and Kumar S 2010 *Phys. Fluids* **22** 023101
[25] Bonn D, Ingremeau F, Amarouchene Y and Kellay H 2011 *Phys. Rev. E* **84** 045301
[26] Pan L, Morozov A, Wagner C and Arratia P E 2013 *Phys. Rev. Lett.* **110** 174502
[27] Perkins T T, Smith D E and Chu S 1997 *Science* **276** 2016
[28] Smith D E, Babcock H P and Chu S 1999 *Science* **283** 1724
[29] Gerashchenko S, Chevallard C and Steinberg V 2005 *Europhys. Lett.* **71** 221
[30] Gerashchenko S and Steinberg V 2006 *Phys. Rev. Lett.* **96** 038304
[31] Groisman A and Steinberg V 2001 *Phys. Rev. Lett.* **86** 934
[32] Burghelea T, Segre E and Steinberg V 2006 *Phys. Rev. Lett.* **96** 214502
[33] Jun Y and Steinberg V 2009 *Phys. Rev. Lett.* **102** 124503
[34] Jun Y and Steinberg V 2010 *Europhys. Lett.* **90** 44002
[35] Thomas D G, Sureshkumar R and Khomami B 2006 *Phys. Rev. Lett.* **97** 054501
[36] Liu N and Khomami B 2013 *J. Fluid Mech.* **737** R4
[37] Berti S, Bistagnino A, Boffetta G, Celani A and Musacchio S 2008 *Phys. Rev. E* **77** 055306
[38] Berti S and Bistagnino A 2010 *Phys. Rev. E* **82** 036314
[39] Zhang H N, Li F C, Cai W H, Yang J C and Li X B 2011 *J. Eng. Thermo.* **32** 973
[40] Thomases B and Shelley M J 2009 *Phys. Rev. Lett.* **103** 094501
[41] Li F C, Zhang H N, Cao Y, Kunugi T, Kinoshita H and Oshima M 2012 *Chin. Phys. Lett.* **29** 94704
[42] Zhang H N, Li F C, Cao Y, Tomoaki K and Yu B 2013 *Chin. Phys. B* **22** 24703
[43] Yu B and Kawaguchi Y 2004 *J. Non-Newtonian Fluid Mech.* **116** 431
[44] Horiuti K and Takagi Y 2001 *Phys. Fluids* **13** 3756
[45] Pope S B 2000 *Turbulent Flows* (Cambridge: Cambridge University Press)